Benha Journal of Applied Sciences (BJAS) **print: ISSN 2356–9751**
Vol. (10) Issue (4) (2025), (101- 113) **online: ISSN 2356–976x**

http://bjas.bu.edu.eg
engineering sciences

Behavior of Hybrid Reinforced Concrete Beams Under Influence of Seawater

Sherif S. Abd el Hamid[1], Amr A. Gamal El Din [1], Ahmed F. Deifalla[2] and Tarik S. El-Salakawy[1]
[1]Civil Engineering Dept., Faculty of Engineering, Shoubra, Benha University
[2]Future University in Engineering, Egypt, Civil Engineering
E-mail: s.abdelhamid60977@feng.bu.edu.eg

Abstract

Reinforced concrete structures in marine environments are vulnerable to deterioration due to chloride-induced corrosion of steel reinforcement. Therefore, this research will study the behavior of hybrid reinforced concrete beams made of rebar steel and glass fiber-reinforced polymers (GFRP) under the influence of seawater by simulating the marine environment using an accelerated corrosion test according to ASTM G31. Nine beams were tested: six were immersed in a corrosive solution, and three were exposed to air. Flexural strength under single-point loading was tested on all specimens after a 45-day accelerated corrosion test. Beams containing silica fume and GFRP bars exhibited increased flexural strength by 5.4% to 16.9% compared to the air-exposed control. In contrast, beams reinforced solely with steel bars showed significant strength losses due to corrosion, ranging from 76.4% to 80.1%, despite the inclusion of corrosion inhibitors in some cases. Hybrid beams also suffered capacity reductions (66.2%–79.9%) due to cracking in the tensile zone, caused by steel corrosion. However, increasing the GFRP ratio in the tension zone clearly improved corrosion resistance and preserved flexural performance. These results highlight the effectiveness of using GFRP reinforcement and supplementary materials such as silica fume and corrosion inhibitors to enhance durability and structural performance in aggressive marine environments. The study supports the development of more corrosion-resistant concrete systems for coastal and offshore applications.

Keywords: accelerated Corrosion, flexural behavior, hybrid bar, load-deflection curve.

1. Introduction

Concrete is one of the oldest and most often used building materials in the world. [1]. A dependable building material for decades, and today no structure can be built without it, consisting of cement, water, aggregate, additives. The types of additives vary based on the specifications and requirements of the project and the surrounding environment with the construction element [2-3]. Due to its moldability, durability, strength, and cost-effectiveness, annual concrete demand for construction is projected to reach 18 billion tons by 2050[4-5]. Concrete is material with a high compressive strength, but a low tensile strength. Thus, concrete reinforcement is required to handle tensile stresses, the traditional reinforcement for concrete structures is steel reinforcement [6-7]. In case of exposure of concrete structures and infrastructure to marine environments continuous or intermittent, leads to corrosion of the steel rebar and deterioration of the concrete as shown in figure (1). So the used material (MCI®-2005) in this research as a corrosion inhibitor to study how resistant is it to protect reinforcing steel from corrosion. The salts present in seawater affect the deterioration of concrete in three ways: physical, chemical, and mechanical, according to some accounting, the average amount of salts is 3.5% [9]. The construction industry has a significant issue with the degradation of reinforced concrete structures due to reinforcement corrosion globally. Because corrosion lead to a reduction in the useful service life of concrete structures exposed to marine environment. Particularly in the Arabian Gulf, where rehabilitating corroded infrastructure can cost billions of dollars. The buildings in the Arabian Gulf only have a 10 to 15-year service life, according to research from the Middle East and Saudi Arabia [10].

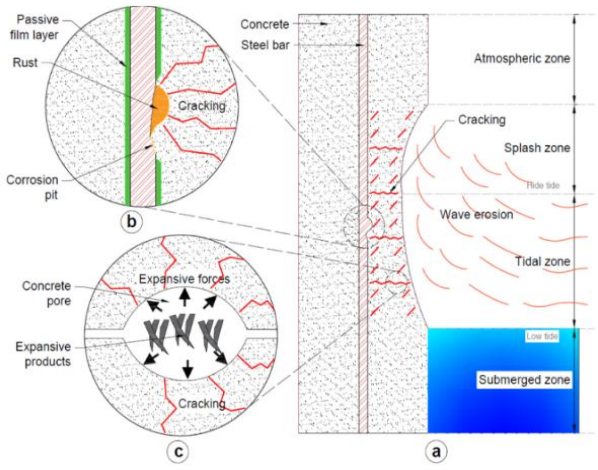

Fig. (1) Deterioration of concrete due to exposure in a marine environment [8].

In recent years, steel rebar is gradually being replaced by non-metallic fiber-reinforced polymer (FRP) technologies. FRP reinforcement is becoming more popular because, in comparison to traditional steel rebar, it has a higher strength-to-weight ratio and is resistant to corrosion [11,12]. Four types of fiber-reinforced polymers (FRP) have been identified based on prior research: Carbon Fiber fiber-reinforced polymer (CFRP), GFRP (glass fiber

reinforced polymer), BFRP (basalt fiber reinforced polymer), and AFRP (aramid fiber reinforced polymer). GFRP (glass fiber reinforced polymer) bars in this research were used because of high corrosion resistance as they are chemically inactive and has a high strength-to-weight ratio compared to conventional steel [13, 14]. However, GFRP bars exhibit a brittle flexural mode of failure compared to steel rebar. On the other hand, steel rebar will tolerate greater levels of ductility than GFRP bars before yielding during permanent deformation. GFRP has a rupture point rather than a yield point, therefor, the failure in flexural concrete structures reinforced using GFRP bars is frequently sudden and unexpected. A proposed solution to overcome these limitations is the combined use of GFRP and steel bars, termed SGFRP reinforcement, as load-bearing reinforcement in flexural concrete structures. By adjusting the content of either the longitudinal reinforcement or GFRP bars, the ductility of beam structures can be enhanced [15-19].

This study investigated the behavior of hybrid reinforced concrete under seawater influence using steel rebar and GFRP bars. Nine concrete beams (130 x 250 x 1300 mm) were manufactured: six subject to accelerated corrosion test (B4S, B5S, B6H, B7H, B8S, and B9S) by electrochemical corrosion and immersion in a 5% sodium chloride solution until surface cracking occurred due to longitudinal reinforcement corrosion, and three exposed to air (B1S, B2S, and B3F). Subsequently, a single-point bending test evaluated the flexural behavior of both corroded and non-corroded beams.

2.0 Experimental program

The experimental work was conducted from the design of the beams, sample preparation, mix design, concrete tests, and corrosion assessment according to the research plan for this study, as shown in figure (2).

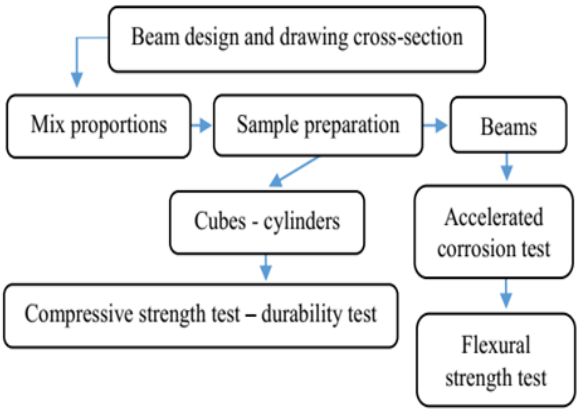

Fig (2) Research Plan Flow Chart

2.1 Mix proportions and Material

Designing a concrete mix means selecting, the suitable proportions of aggregate (fine, coarse), cementitious materials, admixtures, and water, when combined, produce a concrete mixture with the desirable mechanical and physical qualities and properties. In this research, two types of reinforcement were used (GFRP bars, and steel rebar) together to improve corrosion resistance and ductility for hybrid beams. Table 1 shows the mechanical properties of steel bars and GFRP bars, while Fig. (3) illustrates the stress-strain relationship between GFRP and steel reinforcement. Silica fume was added to improve chloride ion ingress resistance to RC and hybrid concrete beams. Steel corrosion inhibitor MCI®-2005 was used to study its effectiveness in protecting the concrete beams made of steel exposed to accelerated corrosion. Four concrete mixtures were designed to investigate their mechanical and durability characteristics for casting the beams utilized in the research, the target compressive strength for the control beam was 40MPa, Table 2 summarizes the concrete mix proportions for concrete.

2.2 Concrete cubes and cylinders tests and results

12 cubes with dimensions of (150 x 150 x 150) mm and 6 cylinders with dimensions of (300 x 150) mm were cast from the mixtures used in casting beams used in this study. The mechanical and durability properties of concrete are investigated through compressive strength test according to BS EN 12390-3 and rapid chloride penetration test according to ASTM C 1202, after 28 days of curing for samples. Tables 3and 4 show the specimen's results.

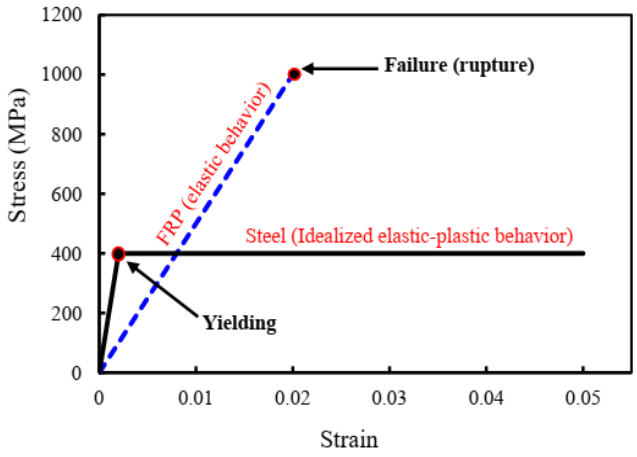

Fig. (3) Stress-strain relationship for GFRP and steel reinforcement [20].

Table (1) Mechanical properties of the steel bars and GFRP bars.

Reinforcement type	Yield strength, f_y (MPa)	Ultimate strength, f_u (MPa)	Ultimate strain
Steel bar Ø10	400	600	0.026
GFRP bar Ø10	——	1027	0.0258

Table (2) Mix proportions of concrete.

Concrete mix components	Type of mix			
	Mix 1	Mix 2	Mix 3	Mix 4
Cement I (kg /m^3)	425	393.125	425	393.125
Coarse Aggregate (kg /m^3)	1150	1150	1150	1150
Fine Aggregate (kg/m^3)	600	600	600	600
Water (l/m^3)	205	195	195	170
Sika Fume (kg/m^3)		31.875		31.875
Sikament (l/m^3)		5.95		5.95
MCI®-2005 (l/m^3)			0.6	0.6

Table (3) Result of the compressive strength test of concrete

Type of mixture and Number of samples		Load (kN)	Compressive Strength (MPa)	increase of strength (%)
Mix 1	3	2591.3	38.3	No additives
Mix 2	3	3295.6	49	27.93 %
Mix 3	3	3003	45	17.49 %
Mix 4	3	4134.7	61	59.26 %

Table (4) Results of the chloride penetration test

Type of mixture and Number of samples		Chloride rapid penetration test ASTM C1202	
		Charge passed (coulombs)	Chloride Ion Penetrability
Mix1	3	3222	Moderate
Mix2	3	532	Very low

2.3 Tested beam samples

Nine concrete beams with dimensions (150 x 250 x 1300 mm) were cast, Fig. (4a, 4b) shows the dimensions and details of the beam's reinforcement, the reinforced with (steel rebar) and hybrid (S-GFRP). Fig. (5a, 5b) also shows the cross-section classification of the beams tested. Fig. (6) shows the beams' preparation, casting, and curing process. The nine test samples were divided as summarized in Table 5:

- Three concrete beams: B1S, B2S, B3F exposed to the air. B1S and B2S were reinforced with steel rebars only. The GFRP bars were used for bottom reinforcement of B3F only while the top reinforcement and stirrups were made of steel reinforcement.
- The other six beams B4S, B5S, B6H, B7H, B8S, and B9S were subjected to accelerated corrosion testing using the electrochemical corrosion method for (rebar) and hybrid (S-GFRP). The sample was immersed in chloride sodium 5% until cracks appeared on the beams' surface due to rebar corrosion.
- Beams B4S, B5S, B8S, and B9S used steel rebar only; beams B5H and B6H utilized GFRP for lower reinforcement and steel bars for upper reinforcement.

Table (5) Details and specifications of test beams

C.B	Mix used	Exposure	Reinforcement		
			Top	Bottom	Stirrups
B1S	Mix 1	Air	2Ø8 (S-S)	3Ø10 (S-S-S)	18Ø8
B2S	Mix 2	Air	2Ø8 (S-S)	3Ø10 (S-S-S)	18Ø8
B3F		Air	2Ø8 (S-S)	3Ø10 (F-F-F)	18Ø8
B4S	Mix 1	Immersed	2Ø8 (S-S)	3Ø10 (S-S-S)	18Ø8
B5S		Immersed	2Ø8 (S-S)	3Ø10 (S-S-S)	18Ø8
B6 H	Mix 2	Immersed	2Ø8 (S-S)	3Ø10 (S-F-S)	18Ø8
B7 H		Immersed	2Ø8 (S-S)	3Ø10 (F-S-F)	18Ø8
B8S	Mix 3	Immersed	2Ø8 (S-S)	3Ø10 (S-S-S)	18Ø8
B9S	Mix 4	Immersed	2Ø8 (S-S)	3Ø10 (S-S-S)	18Ø8
S Denotes for steel bar - F Denotes for GFRP bar					

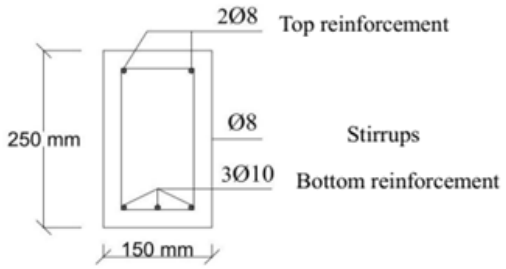

a) Cross section

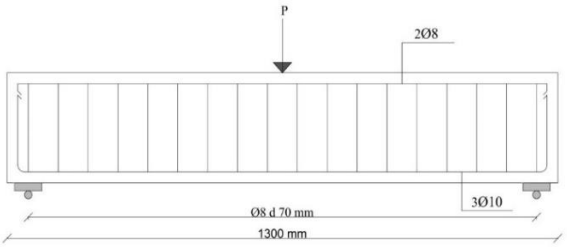

b) Beam reinforcement details: top, bottom, and stirrups

Fig. (4) Beam reinforcement details.

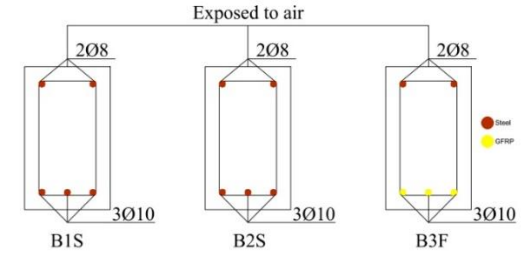

a) Cross-section of beam exposed to air

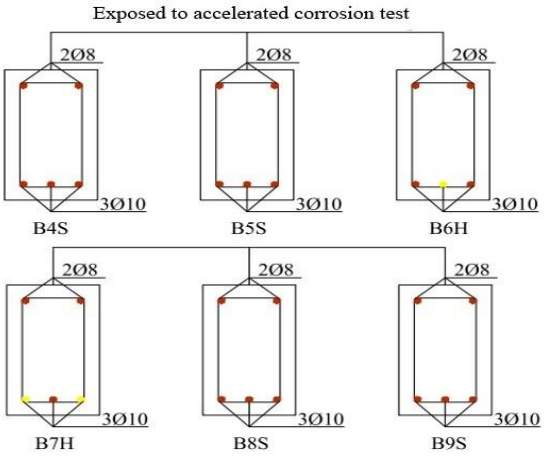

b) Cross-section of beam exposed to accelerated corrosion test

Fig. (5) Classification of beams cross-section.

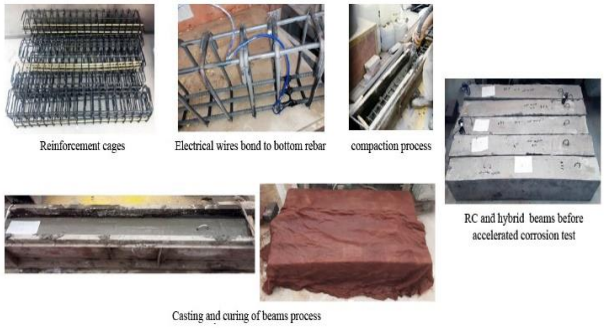

Fig. (6) Preparation, casting, and curing procedures for test beams

2.4 Accelerated corrosion test

Accelerated corrosion testing involves exposing concrete beams to a highly corrosive environment, simulating the effects of many years of natural weathering in a short period. This study aims to evaluate the performance of different types of concrete mixtures and corrosion protection methods to determine their effectiveness in preventing corrosion damage to concrete structures. and comparison between rebar and glass fibre bars in terms of durability. The accelerated corrosion test was applied in this study according to ASTM G31 as shown in Fig. (7). The immersion period of the samples was 45 days, and the steel mass loss was calculated by the weight of the reinforcement cage before and after the corrosion process for each beam, and the test was prepared as follows:

The beams exposed to accelerated corrosion were placed and divided into four plastic basins containing a 5% sodium chloride (NaCl) solution. Then the positive current (+) was connected to the main lower rebar (anode) and the negative current (-) to the stainless-steel metal (cathode) through a DC power supply (24 V). The electrolyte solution was changed every two weeks to keep the constant value of NaCl concentration. The voltage was recorded every week as part of the accelerated corrosion monitoring process. In addition, every two weeks, the beams were lifted from their tanks to observe cracking and inspect the crack's width propagation due to corrosion.

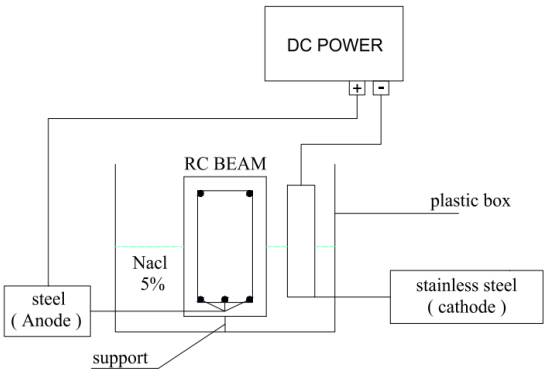

Fig. (7) Accelerated corrosion test according to ASTM G31 [21].

2.5 Single Point-Loading in the Bending Test Setup

After completing the corrosion test, specimens were air-dried, and visual inspection and measurement of cracks due to corrosion were performed. After that, all beams were subjected to a single-point loading bending test using a vertical load at the middle of the span as shown in figure 8 (a, b) the beams were loaded by a hydraulic jack with a loading capacity of 500 tons, the load and retained displacement were recorded automatically using the data accusation system till failure. The load on the beam was measured using a load cell, along with two linear variable differential transformers LVDTs. LVDT(1) and LVDT(2) were positioned at the center of the test specimen to measure beam displacement under load. The maximum deflection of the middle cross-section was determined from these LVDTs measurements.

a) Test setup and apparatus

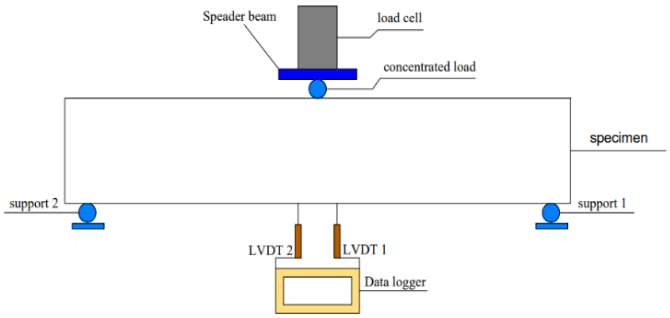

b) Loader parts

Fig. (8) Single Point-Loading of the bending test setup.

3. Inspection of beams and reinforcement after the corrosion process

3.1 Visual inspection of beams after corrosion process

All beams after the corrosion process were visually inspected, evaluating the damage to the submerged beams after the immersion period was ended. Fig. 9 (a, b) shows the status of the beams exposed to corrosion compared to beams exposed to air.

a) non-corroded beam

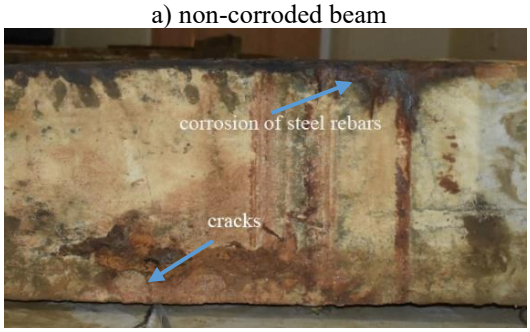

b) Corroded beam

Fig. (9) Visual inspection of beams after corrosion

3.2 External visual inspection of corroded beams

The inspection process includes the external surface and the changes that appear due to the corrosion process such as (cracks, splitting, Surface color change, corroded reinforcement, durability of specimens, etc.) for corroded beams. The rust byproducts, because of their expansion in volume, create internal pressure on the concrete. This pressure leads to cracks in the concrete surrounding the corroding steel due to the concrete's weakness in tension [22-25], causing the concrete to eventually spall away as corrosion progresses, the cracks appeared primarily along the length of steel reinforcement in the tension and compression zones. The result of the examination was as follows:

During the inspection of the immersed beams (B4S, B5S, B6H, B7H, B8S, B9S) post-corrosion process, corrosion of the holder used to lift these beams was observed, also noted that corrosion residues of the steel holder had accumulated on the sides and surface of the beams. Additionally, brown and black stains and cracks on all sides of the beams were identified due to corrosion. Figure 10, divided into a, b, c, and d for each submerged beam, shows the crack patterns on each side of the beam and the locations of corrosion in the upper and lower steel. The numbers on the cracks indicate the width of the crack in each beam in millimeters and was measured using a digital calliper.

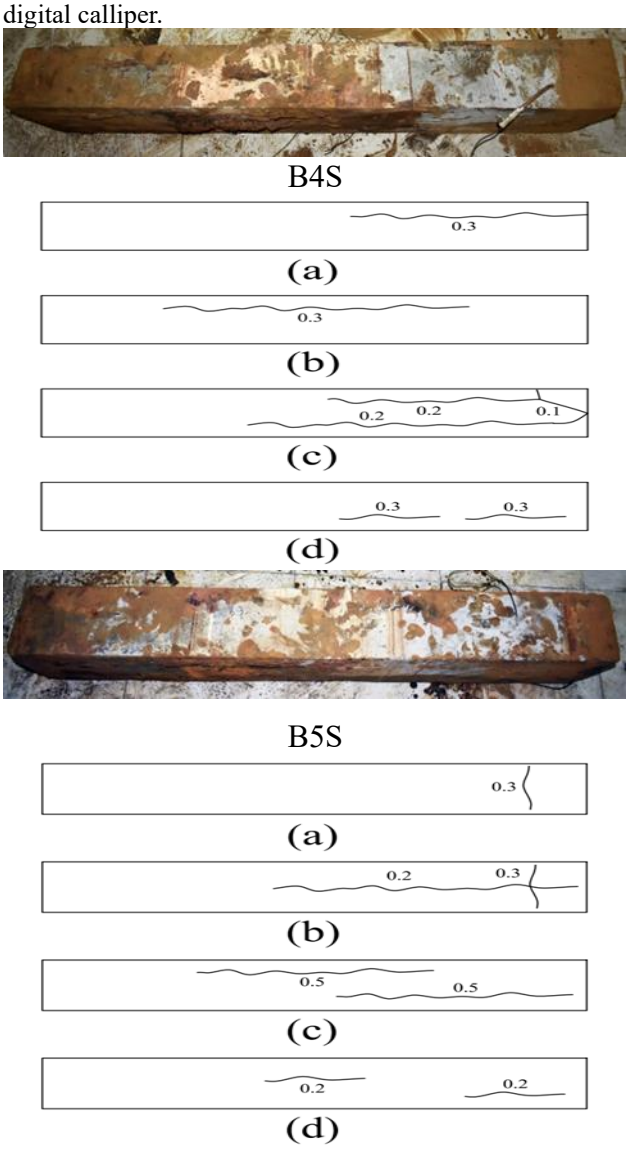

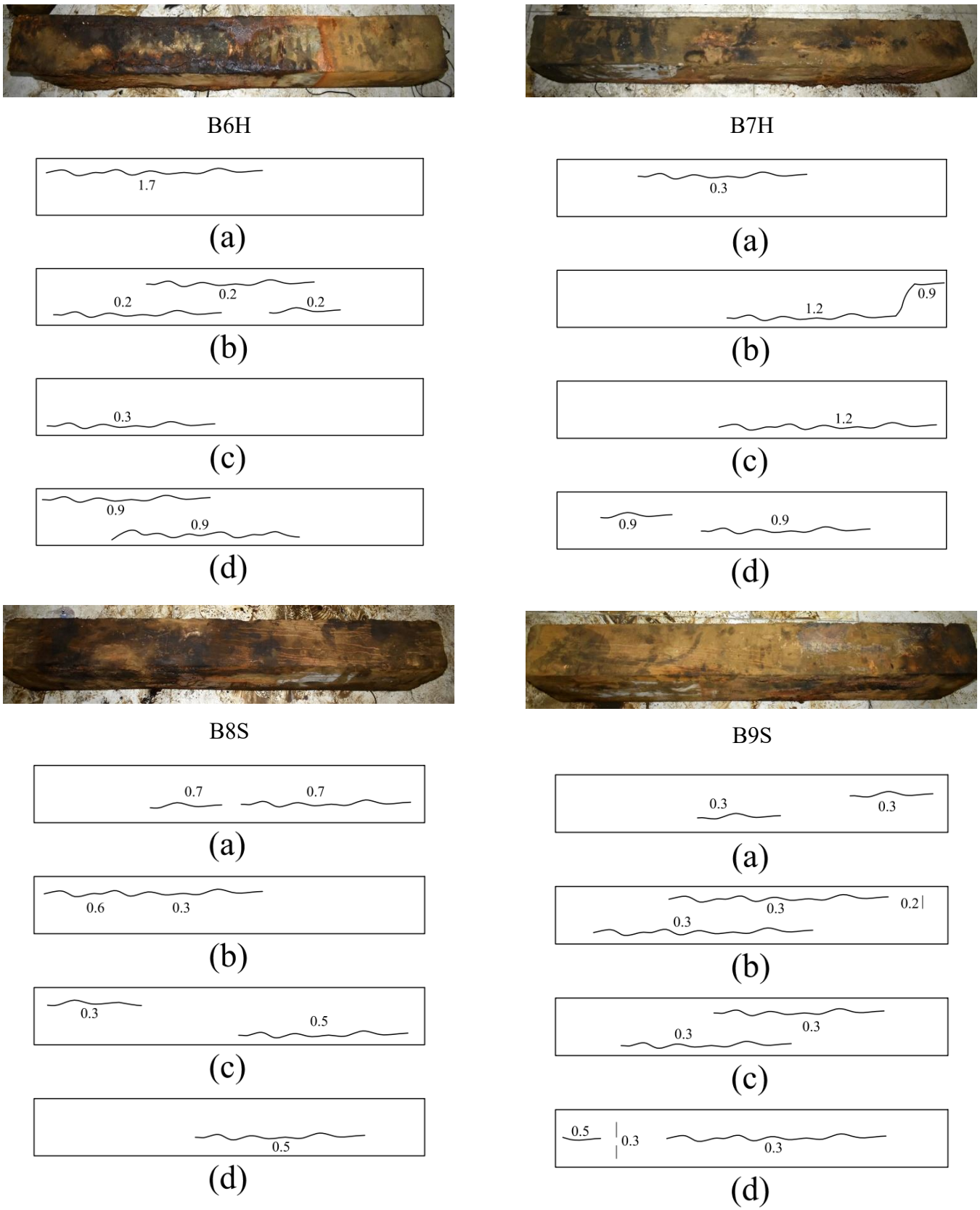

Fig. (10) Maps showing steel corrosion-induced cracks on all sides of test beams.

3.3 Reinforcement inspection for corroded beams

The final internal inspection of the beams includes the following: First, the concrete cover is removed for corroded beams after flexural strength testing to evaluate the condition of the reinforcement visually after the corrosion process compared to non-corroded beams as shown in Fig. 11. Second, the weight of the reinforcement cage in Kg before and after the corrosion process was measured using a digital balance to calculate the weight loss ratio for each beam, as shown in Table 6. After that the actual diameter of the corroded bottom reinforcement was then measured using a digital calliper as shown in Fig. 12.

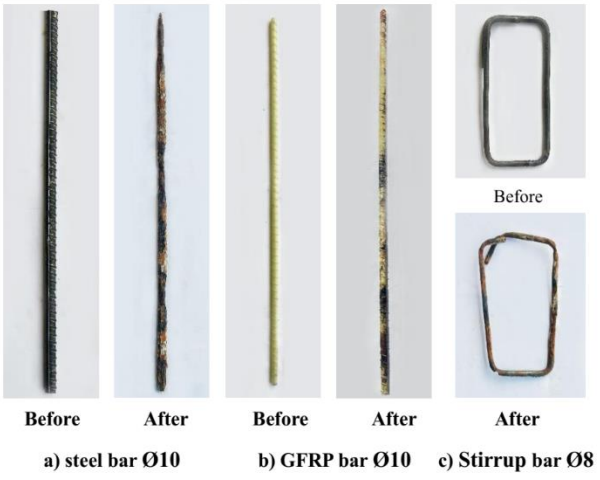

Fig. (11) Steel rebar Ø10 and GFRP bar Ø10 before and after the accelerated corrosion test.

Table (6) weight of the reinforcement cage (Kg) before and after the corrosion process.

Beams	weight before corrosion (Kg)	weight after corrosion (Kg)	Reduction of steel reinforcement (%)
B1S	9.5	Non corroded	
B2S	9.5		
B3F	7.304		
B4S	9.5	5.5	42.10
B5S	9.5	6.54	31.15
B6H	8.868	5.668	36.08
B7H	7.958	6.05	23.97
B8S	9.5	6.23	34.42
B8S	9.5	7.05	25.78

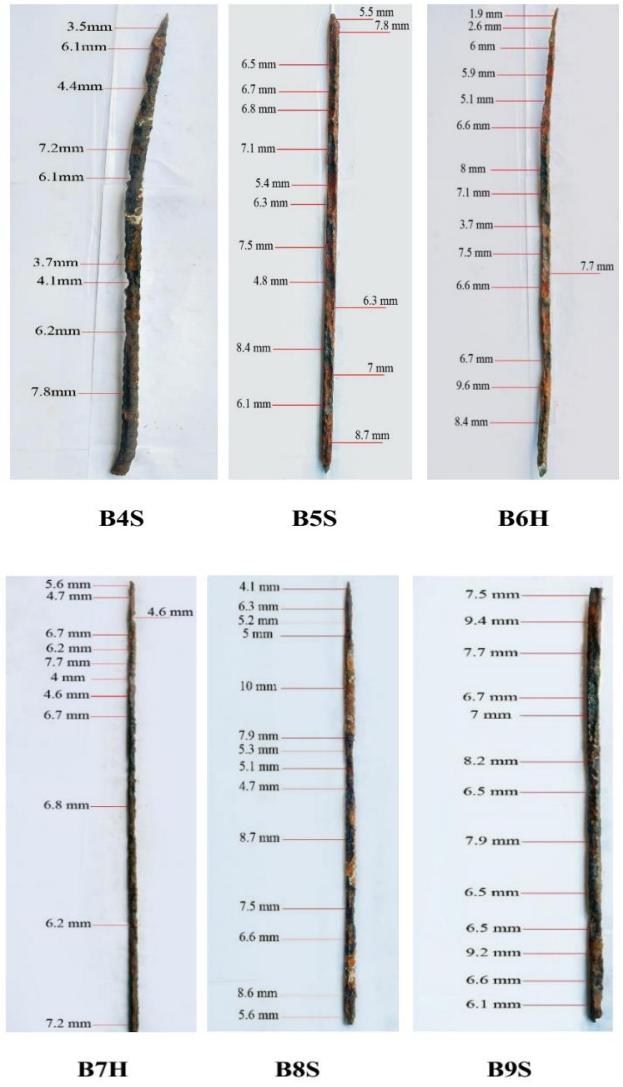

Fig. (12) Actual diameter of bottom reinforcement for the corroded beams.

4. Flexural behavior of test Beams

The flexural behavior of the nine concrete beams was investigated by determining failure loads and ultimate displacements as seen in table 7. Three beams were exposed to air, and the other six underwent an accelerated corrosion test to compare the impact of corrosion on the flexural behavior of hybrid reinforced beams using steel rebar and GFRP bars. Figure 13 illustrates the ultimate failure load and maximum displacement for all beams, while Figure 14 shows the load and displacement curve relationship for each beam. Further explanation and analysis of the various groups is discussed in section 6.

Table (7) Results of the flexural strength test and the failure modes of the beams.

C.B	First crack (kN)	Ultimate failure load (kN)	Maximum displacement (mm)	Failure mode
B1S	51	159.9	38.436	Flexural
B2S	41	168.6	27.466	Flexural
B3F	21	187	28.183	Flexural
B4S	34	34.8	7.668	Flexural and shear
B5S	22	35.5	4.034	Flexural and shear
B6H	14	32.1	10.657	Flexural and shear
B7H	22	54.1	8.72	Flexural and shear
B8S	18	31.8	4.902	Flexural and shear
B9S	28	37.7	4.228	Flexural and shear

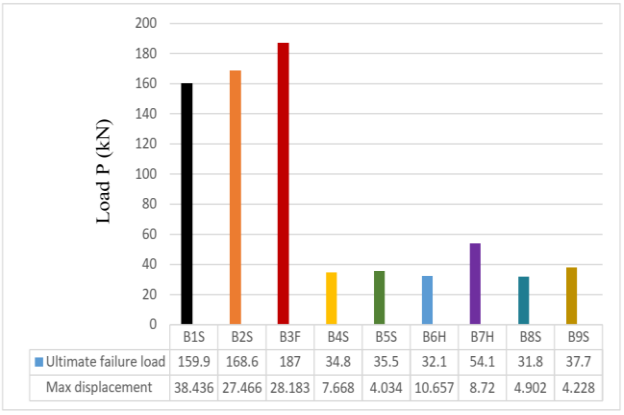

Fig. (13) Ultimate load failure and maximum displacement

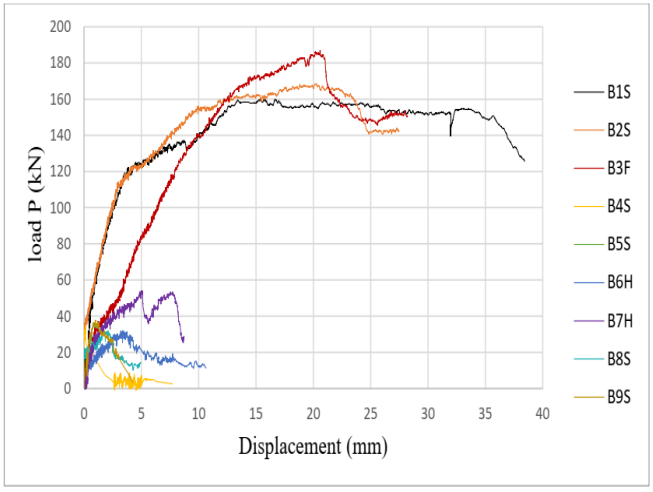

Fig. (14) Load and displacement curve for all specimens

5. Effect of corrosion on beams immersed

Submerged beams (B4S, B5S, B6H, B7H, B8S, and B9S) exhibited lower flexural resistance than the control beam B1S, as shown in figure (15). This reduction was attributed to decreased cross-section in steel rebar due to corrosion as shown in figure (12).

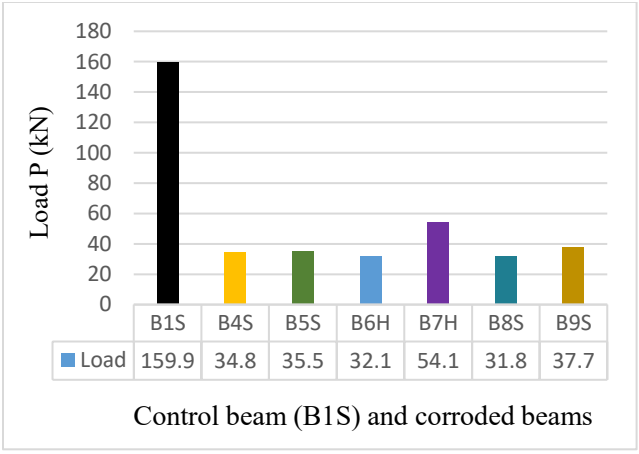

Fig. (15) Effect of corrosion on flexural strength test for corroded beams.

Cohn and Bartlett [26] proposed a more appropriate definition for a displacement ductility index. Based on their definition, the displacement ductility (D) index can be estimated as the ratio of the displacement corresponding to 85% of the maximum load on the post-peak portion of the curve to the displacement corresponding to the first yield displacement of a beam, Δ y the displacement ductility index is the calculated displacement from the load-displacement curve by using the equation (Δ u at 0.85p (max)) / (Δ y) as shown in Fig. 16. Table 8 shows the result of displacement ductility for all beams

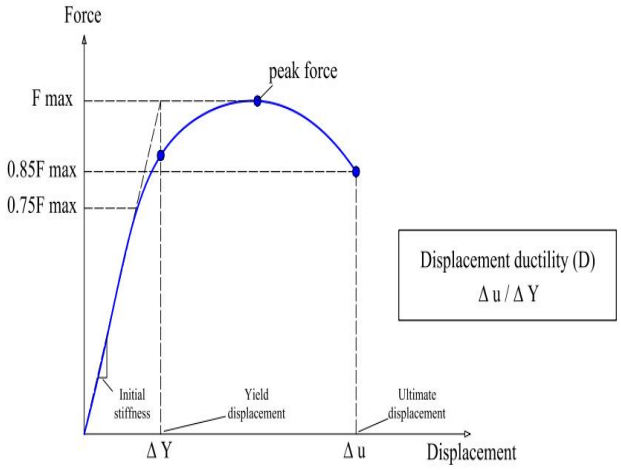

Fig. (16) Displacement ductility curve.

Table (8) Results of displacement ductility.

C.B	Δ_u (mm)	Δ_y (mm)	$\frac{\Delta u}{\Delta y}$	$\frac{(D)beam}{(D)Control}$	mode of failure
B1S	37.5	5	7.5	1	Ductile
B2S	24.63	7.3	3.37	0.449	semi ductile
B3F	22.13	13.2	1.67	0.222	Brittle
B4S					Failure is sudden
B5S	2.2	0.70	3.14	0.418	semi ductile
B6 H	4.24	2.02	2.09	0.278	semi ductile
B7 H	5.14	3.4	1.51	0.201	Brittle
B8S	1.42	0.64	2.21	0.294	semi ductile
B9S	2.4	0.79	3.03	0.404	semi ductile

6. Discussion of the experimental results

This section discusses concrete test results for cubes and cylinders used in the concrete tests. and also present the findings of the flexural strength test and the failure mode, as illustrated in Fig. 17, for all beams exposed to and not exposed to corrosion, and discusses the effect of corrosion on the ductility of steel rebar, and the impact of corrosion on reducing the cross-section steel rebar.

6.1 Concrete test results

compressive strength test results on concrete mixes 1, 2, 3, and 4, shown in Table 3, indicates that mixtures 2, 3, and 4, exhibited improved concrete compressive strength compared to the control mix 1 because they contain silica fume and MCI®-2005 corrosion inhibitor. The improvement rate of the mixtures compared to the control mixture was 27.93%, 17.49%, and 59.26%, respectively. The clear difference in these results is due to the difference in the components of each mixture, as shown in Table 2. From these results, we conclude that the presence of silica fume and steel corrosion inhibitor improves the compressive strength of concrete. Secondly, the chloride penetration test revealed that mix 2, containing silica fume, exhibited 83.48% greater chloride ion ingress resistance than control mix 1, as illustrated in table 4.

6.2 Weight Reduction of Reinforcing Bars after Corrosion

After completing the flexural strength test for all corroded and non-corroded beams, the concrete cover was removed from each corroded specimen, and the remaining steel reinforcement from the corrosion process was extracted for reweighing to determine the percentage of weight loss due to electrochemical corrosion. The original weight of the reinforcement cage was 9.5 kg for beams B4S, B5S, B8S, and B9S, while for beam B6H it was 8.868 kg, and for B7H 7.958 kg, as shown in Table 5. The weight of beams B4S, B5S, B6H, B7H, B8S, and B9S was reduced to 5.5 kg, 6.54 kg, 5.668 kg, 6.05 kg, 6.23 kg, and 7.05 kg, respectively, due to the accelerated corrosion. In other words, the weight loss of the corroded beams decreased by 42.10%, 31.15%, 36.08%, 23.97%, 34.42%, and 25.78%. The examination revealed reinforcement weight loss due to corrosion in steel rebars, but no corrosion in the glass fiber bars was recorded.

6.3 Effect of corrosion on ductility for steel rebar compared to GFRP bars

Despite identical reinforcement, beam B1S exhibited 55.06% greater ductility than B2S, suggesting that the silica fume in B2S reduced its ductility. Beam B3F, reinforced with GFRP bars, exhibited brittle behavior and low ductility by 77.8 % compared to beam B1S, which was reinforced with steel rebar. Because GFRP bars are non-ductile. As for hybrid beams B6H and B7H, they decreased ductility with a ratio of 72.2 % and 79.86%, respectively, compared to beam B1S. This is because of corrosion of the lower steel rebar for hybrid beams. The ductility of the corroded steel beams (B5S, B8S, and B9S) was reduced by 58.2%, 70.62%, and 59.6%, respectively, compared to B1S.

6.4 Load-Displacement Relationship

The B2S beam shows 5.4% higher bearing strength than the B1S beam in bending strength resistance, despite both having the same reinforcement with a maximum displacement of 38.436 mm for B1S and 27,466 mm for B2S. The difference in ultimate failure strength was the existence of silica fume in the B2S. As for B3F the existence of silica fume, along with bottom reinforcement made of GFRP, led to a 16.9% enhancement in bending strength resistance compared to B1S. A maximum displacement for B3F is 28.183 mm, the failure mode cracks naturally propagate, where cracks typically form and spread along the beams tensile. bottom fibers in the midsection and propagate upwards.

The corrosion's effect on flexural strength tests for beams B4S and B5S, compared to beams B1S and B2S exposed to air, shows that B5S has a 2% better bending strength than B4S. B4S has a maximum displacement of 7.668 mm, while B5S has a maximum displacement of 4.034 mm. The bending strengthtest results for both beams highlight the impact of corrosion on ductility due to the deterioration of the main reinforcement and reduction in cross-sectional area. B4S experienced sudden failure due to stirrup corrosion near the shear zone, whereas B5S failure is due to flexure and shear.

Corrosion affected the flexural strength test results for beams B6H-B7H hybrid, showing that beam B7H resistance of flexure strength is better than B6H by 68.5% compared to B1S, due to the increased number of GFRP bars and the inclusion of silica fume in B7H. The beams B6H, and B7H have a maximum displacement of 10.657 mm and 8.72 mm respectively. The failure mode for both beams was a combination of shear and flexural due to the corrosion of stirrups and bottom reinforcement.

In B8S and B9S, a corrosion inhibitor was included to analyze its impact on protecting the reinforcing steel

from corrosion. Upon inspection, corrosion was observed, indicating that this substance merely postpones corrosion rather than halting the chemical processes that lead to it. The B9S beam exhibited 18.5% higher resistance to bending force compared to the B8S beam, B8S should have a maximum displacement 4.902 mm and B9S should have a maximum displacement 4.228 mm. The failure mode in these beams is due to the stirrups' corrosion near the shear zone for B8S. AS for B9S failure mode is flexure and shear.

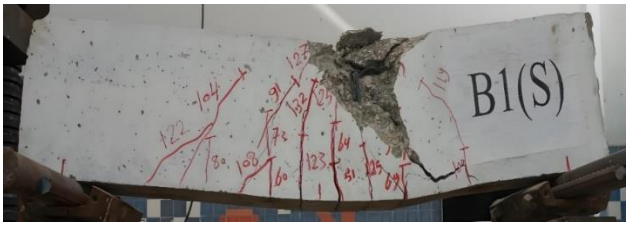

B1S

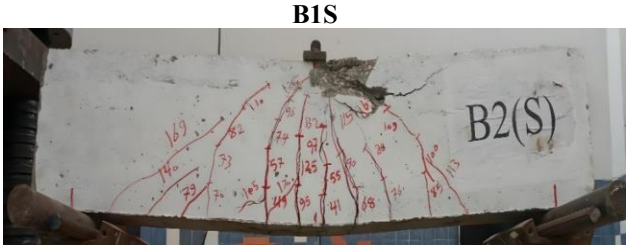

B2S

B3F

B4S

B5S

B6H

B7H

B8S

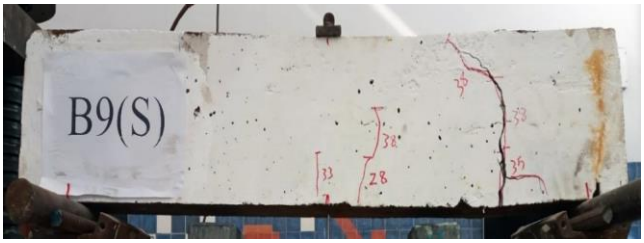

B9S

Fig. (17) Crack patterns on test specimens under flexural test of bottom reinforcement for the corroded beams.

7. Comparison between theory and experiment results

This section compares the flexural capacity of the RC beam and SGFRP hybrid beam between theory and experimental tests for control beam B1S and hybrid B7H. used the strain and stress diagrams for the steel rebar beam and SGFRP beam as illustrated in Fig. 18, and 19, were used to calculate the ultimate moment in comparison with experimental results. Table 9 shows theoretical and experimental results for the critical moment calculation.

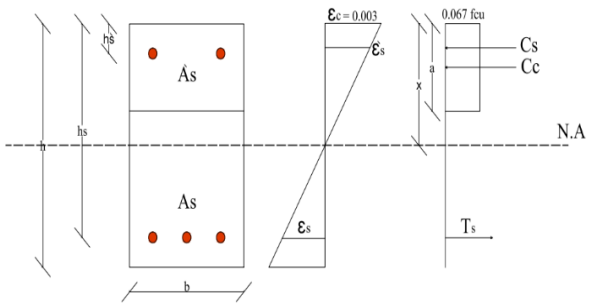

Fig. (18) Diagram of the calculation on the cross-section steel rebar.

Cc=0.67×fcu×a×b [27], Cs= E_S×A′s×ε′s, Ts= E_S×As×εs

Cc+Cs=Ts ⟶ Equilibrium equation

0.67×fcu×a×b+ E_S×A′s×ε′s= E_S×As×εs (1) ∴

Take a= 0.8X

Get X from equation (1)

Calculation Mu (ultimate moment) from this equation:

$$Mu = Cs\left(h's - \frac{X}{2}\right) + Ts\left(hs - \frac{X}{2}\right) \quad (2)\ [26].$$

- NOTES (1)

Cc (concrete in the compression zone), Cs (compressive reinforcement), Ts (tensile reinforcement), As (area of tensile reinforcement), A′s (area of compressive reinforcement).

- NOTES (2)

Assuming that the concrete is perfectly bonded to the reinforcement and ignoring the contribution of concrete in the tension zone, the deformation values for compressive reinforcement, and tension reinforcement are determined using this equation [27]:

$$\varepsilon's = E_S \times A's \times \frac{X - h's}{X} \times \varepsilon c \ , \ \varepsilon s = E_S \times As \times \frac{hs - X}{X} \times \varepsilon c$$

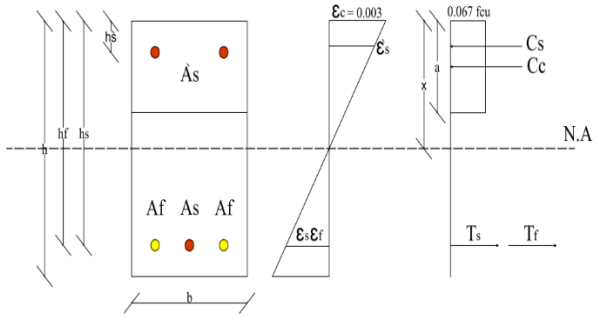

Fig. (19) Diagram of the calculation on the cross-section of SGFRP beam.

Cc=0.67×fcu×a×b, Cs= E_S×A′s×ε′s, Ts= E_S×As×εs, T_f = Ef×Af×εf

Cc+Cs=Ts+T_f ⟶ Equilibrium equation

0.67×fcu×a×b+ES×A′s×ε′s= E_S×As×εs+Ef×Af×εf (1)

∴ Take a= 0.8X

Get X from equation (1)

Calculation Mu (ultimate moment) from this equation:

$$Mu = Cs\left(h'_s - \frac{X}{2}\right) + Ts\left(h_s - \frac{X}{2}\right) + T_f\left(h_f - \frac{X}{2}\right) \quad (2)\ .$$

- NOTES (1)

Cc (concrete in the compression zone), Cs (compressive reinforcement), Ts (tensile reinforcement), T_f (GFRP reinforcement), As (area of tensile reinforcement), A′s (area of compressive reinforcement), Af (area of GFRP reinforcement) .

- NOTES (2)

Assuming that the concrete is perfectly bonded to the reinforcement and ignoring the contribution of concrete in the tension zone, the deformation values for compressive reinforcement, and tension reinforcement, and GFRP bar are determined using these equations:

$$\varepsilon's = E_S \times A's \times \frac{X - h's}{X} \times \varepsilon c \ , \ \varepsilon s = E_S \times As \times \frac{hs - X}{X} \times \varepsilon c$$

$$, \ \varepsilon f = E_f \times Af \times \frac{hf - X}{X} \times \varepsilon c$$

Table (9) Comparison of theoretical and experimental results for the critical moment calculation

Test specimen	Theoretical result (kN.m)	Experimental result (kN.)
B1S	50.89	51.96
B7H	20.91	17.58

Conclusions

This experimental study investigated the flexural behavior of hybrid steel-GFRP rebar beams after accelerated corrosion, focusing on the detrimental effects of seawater on steel-reinforced versus GFRP-reinforced elements. The main conclusions are:

1. Beams B2S (with silica fume) and B3F (with silica fume and GFRP bars) exposed to air exhibited superior flexural strength compared to the control beam B1S, showing increases by 5.4% and 16.9%, respectively. This improvement is attributed to the presence of silica fume in B2S, while both silica fume and GFRP bars contributed to the enhanced flexural strength of B3F.
2. Beams reinforced solely with steel bars (B4S, B5S, B8S, and B9S) showed a decrease in flexural strength due to accelerated corrosion, with a ratio of 78.23%, 77.79%, 80.11%, and 76.42%, respectively, compared to beam B1S. The best performance achieved was that of beam B9S due to the existence of silica fume and MCI 2005 corrosion inhibitor.
3. Compared to beam B1S, flexural strength reductions of 79.92% and 66.16% were observed in hybrid beams B6H and B7H, respectively, due to concrete cracking in the tensile zone caused by reinforcement corrosion. Increasing the GFRP bar ratio improved corrosion resistance of the bottom reinforcement in B7H.

4. Steel corrosion inhibitor delays corrosion and reduces damage, it does not eliminate it. This is demonstrated by the flexural strength reduction of beams B8S and B9S by (80.11% and 76.42%, respectively) compared to B1S.
5. The ductility of the hybrid corroded beams (B6H and B7H) was 72.2% and 79.86%, respectively, compared to B3F.Which indicates the effectiveness of GFRP bars in corrosion resistance.
6. The theoretical calculation of the ultimate moment for control beam B1S was 50.89 kN.m, while the experimental result was 51.96 kN.m. The difference between these results was minimal, by 2.1%. As for hybrid beam B7H, the theoretical calculation of the ultimate moment was 20.91 kN.m, while the experimental result was 17.58 kN.m. The difference between these results was 19 %. Due to the effect of the corrosion process.

Compliance with Ethical Standards:

The authors declare that they have no conflict of interest.

Data availability statement (DAS)

The datasets generated during and/or analyzed during the current study are available from the corresponding author on reasonable request.

Reference

[1] Li, Z. "Advanced Concrete Technology," John Wiley & Sons, Inc., 2011.
[2] Mangi, S.A., Wan Ibrahim, M.H., Jamaluddin, N., Arshad, M.F., Ramadhansyah, P.J. "Effects of ground coal bottom ash on the properties of concrete," J Eng Sci Technol, 14(1):338–350, 2019.
[3] Ali, M.F., Memon, N.A., Memon, B.A., Memon, M.A., Memon, A.N. "The effect of textile on compressive strength of concrete," Quest Res J, 17(2):21–26, 2019.
[4] Jatoi, M.A., Solangi, G.S., Shaikh, F.A., Khan, S., Ahmed, S. "Effect of Lakhra fly ash as partial replacement of cement in traditional concrete," Mehran Univ Res J Eng Technol, 38(4):1045–1056, 2019. https://doi.org/10.22581/muet1982.1904.16.
[5] Mangi, S.A., Wan Ibrahim, M.H., Jamaluddin, N., Arshad, M.F., Memon, F.A., Jaya, P.R., Shahidan, S. "A review on potential use of coal bottom ash as a supplementary cementing material in sustainable concrete construction," Int J Integr Eng, 10(9):127–135, 2018.
[6] Tantawi, H.M. "Ultimate Strength of Highway Girder Bridges," Ann Arbor: University of Michigan, 1986.
[7] Nowak, A., Al-Zaid, R., Hong, Y.-K., Kayser, J., Tabsh, S., Tantawi, H.M., Zhou, J.-H. "Risk analysis for evaluation of bridges," Report UMCE 88-5, University of Michigan, Ann Arbor, 1988.
[8] Mehta, P.K., Monteiro, P.J. "Concrete Microstructure, Properties and Materials," The McGraw-Hill Companies, Inc, 2006.
[9] Islam, M.S., Islam, M.M., Mondal, B.C. "Effect of freeze-thaw action on physical and mechanical behavior of marine concrete," J Inst Eng Malaysia, 71(1):53–64, 2010.
[10] Imam, A. "Shear strength of corroded reinforced concrete beams," MS Thesis, King Fahd University of Petroleum and Minerals, Dhahran, Saudi Arabia, 2012.
[11] Almusallam, T.H., Al-Salloum, Y.A., Alsayed, S.H., Mosallam, A.S. "Durability and long-term behavior of reinforced concrete beams strengthened with FRP composites," In Proceedings of International Conference on FRP Composites in Civil Engineering (CICE 2001), Hong Kong, China, 12–15 December 2001; pp. 1579–1588.
[12] Micelli, F., Nanni, A. "Durability of FRP rods for concrete structures," Constr. Build. Mater., 18, 491–503, 2004.
[13] Zhu, H., Li, C., Cheng, S., Yuan, J. "Flexural Performance of Concrete Beams Reinforced with Continuous FRP Bars and Discrete Steel Fibers under Cyclic Loads," Polymers, 14(2022):1399. https://doi.org/10.3390/polym14071399.
[14] Fan, X., Zhang, M. "Experimental study on flexural behavior of inorganic polymer concrete beams reinforced with basalt rebar," Compos. Part B Eng., 93:174–183, 2016. https://doi.org/10.1016/j.compositesb.2016.03.021.
[15] Jia, B., Liu, S., Liu, X., Wang, R. "Flexural capacity calculation of hybrid bar reinforced concrete beams," Materials Research Innovations, 18(suppl2), S2-836–S2-840, 2014. doi:10.1179/1432891714Z.000000000498.
[16] Lau, D., Pam, H.J. "Experimental study of reinforced concrete beams," Engineering Structures, 32(12):3857–3865, 2010. doi: 10.1016/j.engstruct.2010.08.028.
[17] Mahmoud, A., Nasser, M., Mostafa, T., Khater, A. "Retrofitting of Box Section Concrete Beams to Resist Shear and Torsion Using Near-Surface-Mount (NSM) GFRP Stirrups," Fracture and Structural Integrity, 18(67):319–336, 2023. https://doi.org/10.3221/IGF-ESIS.67.23.
[18] Ifrahim, M.S., Sangi, A.J., Ahmad, S.H. "Experimental and numerical investigation of flexural behaviour of concrete beams reinforced with GFRP bars," In Structures, Vol. 56, p. 104951, Elsevier, 2023. https://doi.org/10.1016/j.istruc.2023.104951.
[19] Mansour, M.A.N., Mustafa, T.S., Khater, A.N. "Innovative Strengthening of Shear and Torsion Performance in Box-Section Concrete Beams with Near-Surface Mounted GFRP Rods," Engineering

Research Journal (Shoubra), 54(1):183–196, 2025. https://dx.doi.org/10.21608/erjsh.2024.341303.1382.

[20] Ibrahim, H.A., Wu, Z., Fahmy, M.F.M. "3D FE ANALYSIS FOR THE SEISMIC BEHAVIOR OF HYBRID STEEL-FRP REINFORCED CONCRETE BEAM-COLUMN JOINTS," 2017. https://www.researchgate.net/publication/328583173

[21] Bhalgamiya, S., Tivadi, G., Jethva, M. "Techniques for accelerated corrosion test of steel concrete for determine durability," ISO 9001:2008 Certified Journal: 4399–4402, 2018.

[22] Al-Harthy, A., Stewart, M.G., Mullard, J. "Concrete cover cracking caused by steel reinforcement corrosion," Magazine of Concrete Research, 63(9):655–667, 2011. doi:10.1680/macr.2011.63.9.655.

[23] Fang, C., Lundgren, K., Chen, L., Zhu, C. "Corrosion influence on bond in reinforced concrete," Cement and Concrete Research, 34(11):2159–2167, 2004. doi: 10.1016/j.cemconres.2004.04.006.

[24] Zhou, Y., Zheng, Y., Sui, L., Hu, B., Huang, X. "Study on the flexural performance of hybrid reinforced concrete beams with a new cathodic protection system subjected to corrosion," Materials, 13(1):234, 2020. https://doi.org/10.3390/ma13010234.

[25] Nguyen, T.H., Nguyen, V.T. "Experimental study on the flexural behaviour of corroded concrete beams reinforced with hybrid steel/GFRP bars," Structure and Infrastructure Engineering, 2022. https://doi.org/10.1080/15732479.2022.2123530.

[26] Cohn, M.Z., Bartlett, M. "Computer-simulated flexural tests of partially pre-stressed concrete sections," ASCE Journal of Structural Division, 108(ST12):2747–2765, 1982.

[27] Egyptian Code for Design and Construction of Concrete Structures ECP 203-2020.